

Synthesis, crystal structure and magnetic properties of a novel nitroxide biradical. Theoretical investigation of the exchange mechanisms

Jörg Fritscher, Mario Beyer, Olav Schiemann *

*Institut für Physikalische und Theoretische Chemie, Johann Wolfgang Goethe-Universität Frankfurt, Marie-Curie-Str. 11,
D-60439 Frankfurt am Main, Germany*

Received 1 July 2002; in final form 21 August 2002

Abstract

The novel nitroxide biradical 1,8-bis(3-ethynyl-2,2,5,5-tetramethyl-3-pyrroline-1-oxyl)-naphthalene was synthesized and its structure and magnetic properties were investigated. Using SQUID measurements an antiferromagnetic exchange coupling of $2J = -3.5$ K was evaluated. Temperature-dependent measurements of the half-field EPR signal intensity and broken symmetry DFT computations confirm this result. To unravel the mechanisms of the intramolecular exchange interaction calculations on model systems were performed. These revealed a strong ferromagnetic through-bond interaction via the 1,8-substituted naphthalene bridge and a competing strong antiferromagnetic through-space interaction via the acetylene groups. Both interactions are of the same order of magnitude leading to the weak overall coupling observed.

© 2002 Elsevier Science B.V. All rights reserved.

1. Introduction

The basis for bulk and molecular magnetic phenomena is the electron spin–spin exchange coupling between unpaired electrons localized on different centers. The correlation of this exchange coupling with structural parameters of the inquired system is a long-standing research topic [1]. Therefore, a lot of experimental and theoretical studies have been devoted to the dependence of the exchange coupling upon structural parameters, leading for example to the conclusion that the exchange coupling constant

J decreases exponentially with the distance [2] and that it depends on the orientation of the magnetic orbitals with respect to each other [3]. In addition, the importance of the geometry and nature of the bridge connecting the paramagnetic centers for the intramolecular interaction was notified [4,5]. However, the acquired knowledge does not yet allow an unequivocal understanding of the distance and orientation dependence of the magnetic interaction. One reason for that may be that the experimentally measured exchange coupling constant J is the result of a superposition of various mechanisms [5]. As Barone et al. [6] showed before, a quantum chemical approach to separate the different through-space and through-bond contributions from each other can be a way to contribute to a deeper understand-

* Corresponding author. Fax: +49-69-79-82-9404.

E-mail address: o.schiemann@prisner.de (O. Schiemann).

ing of the mechanisms driving the magneto-structural correlations.

One powerful and widely used concept to synthesize exchange-coupled biradicals is to connect paramagnetic transition metal complexes [7,8] or organic free radicals [9,10] via organic or inorganic bridges. Within the group of organic free radicals nitroxides have the advantage that they are stable and can be easily handled and derivatized.

Here we present the synthesis and crystal structure of the novel bisnitroxide 1,8-bis(3-ethynyl-2,2,5,5-tetramethyl-3-pyrroline-1-oxyl)-naphthalene $2^{\bullet\bullet}$ (BITPAN, Fig. 1a), its magnetic properties obtained from SQUID and electron paramagnetic resonance (EPR) measurements as well as from broken symmetry (BS) density functional theory (DFT) computations. Furthermore, we show the theoretical separation of the through-bond and through-space mechanisms contributing to the measured exchange interaction.

2. Theoretical background

To describe magnetic exchange interactions in biradicals the phenomenological Heisenberg–Dirac–van Vleck (HDVV) spin Hamiltonian [5]

$$\hat{H}_J = -2J\hat{S}_a\hat{S}_b \quad (1)$$

is used. Here, \hat{S}_a and \hat{S}_b are the total spin operators of the two magnetic centers and J is the exchange coupling constant defined as

$$E_S - E_{S-1} = -2JS, \quad (2)$$

where E_S is the energy of a state with total spin S . $J < 0$ represents an antiferromagnetic (singlet ground state) and $J > 0$ a ferromagnetic (triplet ground state) coupling of the electron spins.

One way to determine J experimentally is to measure the magnetic susceptibility χ at various temperatures T and to fit the data by means of the Bleaney–Bowers equation [11]

$$\chi = \frac{2Ng^2\mu_B^2}{kT} \left(\frac{1}{3 + \exp(-2J/kT)} \right), \quad (3)$$

where μ_B is the Bohr magneton, N is Avogadro's number, g is the electronic Zeeman factor and k is Boltzmann's constant. Best fits of $\chi = f(T)$ to Eq. (3) yield the sign and absolute size of the coupling. In a similar way temperature-dependent continuous wave (cw) EPR experiments can be analyzed to extract J . In this case χ has to be substituted by the measured doubly integrated EPR signal intensity I at different temperatures and $2Ng^2\mu_B^2/k$

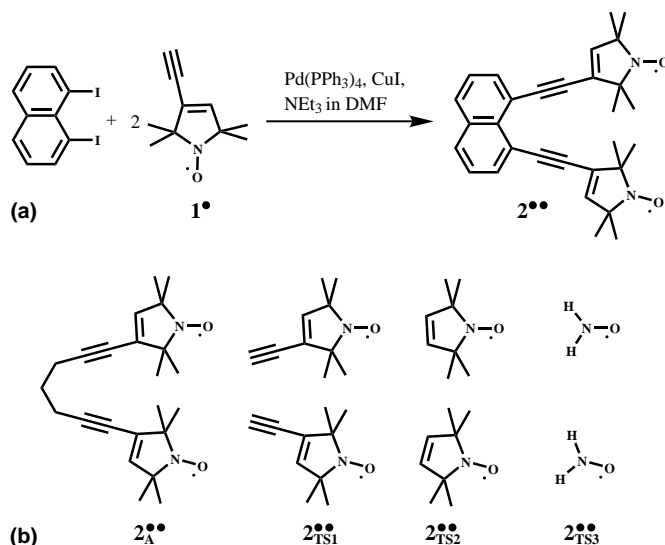


Fig. 1. (a) Reaction scheme for the synthesis of $2^{\bullet\bullet}$. (b) Structures of model systems used in the theoretical evaluation of the exchange mechanisms for $2^{\bullet\bullet}$.

must be substituted by a spectrometer constant C [12].

The computation of the exchange coupling parameter J is a theoretically demanding task as the accurate description of the ground and low-lying excited states in exchange-coupled systems requires the use of multiconfigurational wave functions which is only feasible for small systems at the post-SCF ab initio level. Therefore, alternative approaches, like DFT [13], have to be used for magneto-structural correlations on real chemical compounds. Whereas the highest spin state of a system can be represented by a single determinant and thus be easily treated by Kohn–Sham DFT, this is not the case for the other spin states [14]. Several studies have shown that the latter cases can be handled by evaluating the energy of a fictive electronic state lying between the low- and high-spin eigenstates of the \hat{S}^2 operator [14]. This state is referred to as the BS state [15] and corresponds to a Slater determinant built-up with orbitals localized on the different magnetic centers bearing electrons with opposite spin [16]. To correlate the BS state with a low-spin eigenstate of the HDVV Hamiltonian and to calculate the exchange coupling constant J different methods can be used. The BS formalism [15], the spin projection technique of Ovchinnikov and Labanowski [17] as well as the method described by Yamaguchi and co-workers [18] use spin-projected formulas for the evaluation of J from the energies of the high-spin and BS state whereas other authors assume that the BS energy adequately mirrors that of the low-spin state [19].

Following the rather general formalism of Ovchinnikov and Labanowski [17] one obtains for a system of two active electrons the following expression for the exchange coupling constant J , i.e., for the singlet–triplet splitting $2J$:

$$2J = E_S - E_T = \frac{E_{BS} - E_T}{1 - b^2} \quad (4)$$

with

$$b^2 = \frac{1}{2} \langle \Psi_{BS} | \hat{S}^2 | \Psi_{BS} \rangle. \quad (5)$$

When the BS state is a simple average of the singlet and the triplet state (non-overlapping magnetic

orbitals), i.e., for $\langle \Psi_{BS} | \hat{S}^2 | \Psi_{BS} \rangle \approx 1$, this equation reduces to the original result of Noodleman [15]

$$2J = 2(E_{BS} - E_T), \quad (6)$$

which was used for all computations of J in this work.

3. Computational details

All calculations were performed with the GAUSSIAN 98 program package [20] together with the standard split valence 6-31G(d), 6-31+G(d), 6-31+G(d,p), 6-311G(d), 6-311+G(d), 6-311G(d,p) and 6-311G(df,pd) basis sets [21]. The energies of the different spin states of 2^{\bullet} were computed using the unrestricted Kohn–Sham formalism [13] with the popular B3LYP hybrid functional [22,23]. The geometry of 2^{\bullet} used for all calculations was taken from the crystal structure analysis (see Section 4.1). In the applied structural model potential intermolecular interactions are neglected (see Section 6). The expectation values of the \hat{S}^2 operator, $\langle \hat{S}^2 \rangle$, were checked for all wave functions obtained in these studies to be sure that the use of Eq. (6) was justified in all cases and that erroneous results due to spin contamination artefacts could be avoided.

4. Experimental results

4.1. Synthesis and crystal structure

Chemical synthesis under argon was carried out in Schlenck technique. 3-ethynyl-2,2,5,5-tetramethyl-3-pyrroline-1-oxyl (TPA) 1^{\bullet} [24] and 1,8-diiodonaphthalene [25] were synthesized according to literature procedures.

2^{\bullet} was synthesized from 1^{\bullet} and 1,8-diiodonaphthalene via a Sonogashira cross-coupling reaction using tetrakis(triphenyl-phosphine)-palladium(0) (Pd(PPh₃)₄) and copper(I)-iodide (CuI) as the catalysts and triethylamine (NEt₃) as the base (see Fig. 1a). 125 mg (0.76 mmol) of 1^{\bullet} and 859 mg (2.26 mmol) of 1,8-diiodonaphthalene were mixed in 50 ml of dimethylformamide (DMF) and repeatedly evacuated and loaded with argon.

After addition of 132 mg (0.11 mmol) of $\text{Pd}(\text{PPh}_3)_4$ and of 290 mg (1.53 mmol) of CuI the mixture was evacuated and loaded with argon once again. Then 73 mg (0.72 mmol) NEt_3 were added and the mixture was stirred for 6 h at 25 °C. Volatile components of the grey–brown solution were removed under reduced pressure, the residue dissolved in a solution of $\text{MeOH}:\text{CH}_2\text{Cl}_2$ 1:4 and filtered over silica gel. The filtrate was concentrated in vacuo and separated via column chromatography using toluene as the eluent. The crude product was recrystallized from toluene at 0 °C and afforded pure **2**^{••} as orange monoclinic crystals. Yield: 200 mg (0.88 mmol), 20%. Anal. calcd. for $\text{C}_{30}\text{H}_{32}\text{N}_2\text{O}_2$: C, 79.55; H, 7.13; N, 6.19. Found: C, 80.02; H, 7.12; N, 6.22. ESI-MS(M^+) in MeOH calcd.: 452.6 g/mol; found 453.3 (85%, M^+), 470.3 (100%, $\text{M}^+ + \text{OH}$). The crystals were suitable for X-ray diffraction. Structure data were collected by means of a STOE IPDS system employing Mo K_α radiation ($\lambda = 0.71073 \text{ \AA}$). Crystal data for **2**^{••}: monoclinic space group $P2_1/n$, $Z = 4$, $a = 6.885(2) \text{ \AA}$, $b = 15.228(4) \text{ \AA}$, $c = 24.578(5) \text{ \AA}$, $\alpha = 90^\circ$, $\beta = 93.230(10)^\circ$, $\gamma = 90^\circ$, R indices (all data) $R1 = 0.0971$, $wR2 = 0.1150$. The structure of **2**^{••} in the crystal is displayed in Fig. 2. The structural parameters for the two TPA units in **2**^{••} are similar and comparable to those of **1**[•] [26]. The N–O bond length is 1.27 Å and the N–O vectors are in plane with the planar five-membered ring as in free **1**[•]. The C16/C17 and C13/C14 bonds are C–C single bonds with lengths of 1.49 and 1.52 Å, respectively, whereas C17 and C13 are connected via

a double bond of 1.32 Å length. The C13/C12 and C11/C1 bonds are with 1.42 and 1.44 Å, respectively, significantly shorter than C–C single bonds indicating a conjugation with the C12/C11 triple bond of 1.19 Å length. The distance between the acetylene units amounts to 2.89 and 3.56 Å for C11/C31 and C12/C32, respectively. A dihedral angle of 7.9° for C12/C11/C31/C32 indicates that the triple bonds are almost in-plane enabling π – π -orbital interactions. The naphthalene ring itself is planar and all C–C bond lengths are between single and double bonds. Therefore a conjugated π -system from the double bond in one nitroxide ring via the acetylene group through the naphthalene ring up to the second acetylene group and into the double bond of the second nitroxide ring is built up in **2**^{••}. The rotation of 10.7° and 83.9° of the nitroxide rings out of the naphthalene plane does not disrupt the conjugation due to the almost cylindrical symmetry of the two π -orbitals around the C–C triple bond. However, both N–O groups are separated from this π -system by a C–C and a C–N single bond.

The rotation of the pyrroline rings out of the naphthalene plane leads to an almost perpendicular arrangement (73.3°) of the two five-membered rings with respect to each other. Furthermore, one TPA arm is bent above (9°) and the other below (4°) the naphthalene plane and the vectors C1–C13 and C3–C33 open up an angle of 29.7°. In addition the two acetylene linkers are not linear but display angles of 173.0° and 168.4° for C1–C11–C12 and C3–C31–C32, respectively, and of 176.5° and

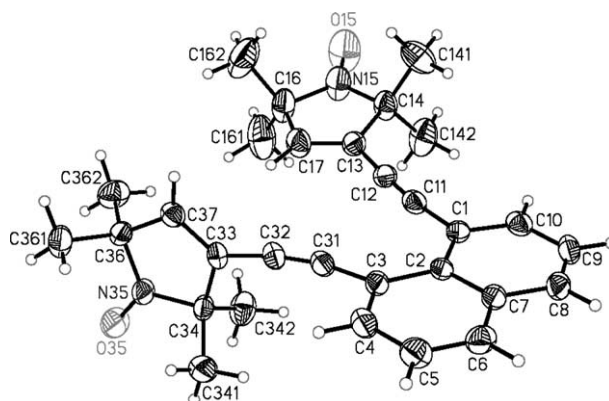


Fig. 2. ORTEP drawing of **2**^{••} showing 50% probability thermal ellipsoids for all non-hydrogen atoms.

172.1° for C11–C12–C13 and C31–C32–C33, respectively. These distortions are attributed to the steric hindrance between the methyl groups and the five-membered rings.

Finally, the through-space distance between the oxygen atoms of the two N–O groups amounts to 8.9 Å and the distance between the nitrogen atoms to 7.2 Å.

4.2. EPR measurements

The cw S-band EPR spectrum was recorded on a home-built cw/pulsed EPR spectrometer using a bridged loop gap resonator equipped with a helium cryostat (CF935) from Oxford as specified previously [27]. The cw X-band EPR spectra were acquired on a Bruker ESP300E EPR spectrometer using a standard rectangular ER4102T cavity from Bruker equipped with a helium cryostat (ESR900) from Oxford. The G-band EPR spectrum was measured in transmission mode on a home-built EPR spectrometer as specified in [28].

For all measurements 1 mM solutions of **1**[•] or **2**[•] in *d*₈-toluene were used. The shown simulations were done with the XEMR program [29].

The isotropic cw X-band EPR spectrum of **1**[•] displays the three lines from isotropic hyperfine coupling to one nitrogen (*I* = 1). Its anisotropic cw G-band EPR spectrum (*T* = 10 K) visualized in Fig. 3a shows a fully resolved *g* tensor as well as the *A*_{zz} component of the nitrogen hyperfine coupling tensor. From the simulations of both spectra the following EPR parameters could be obtained: *g*_{iso} = 2.0063(1), *A*_{iso} = 14.3(1) G, *g*_{xx} = 2.0097(1),

*g*_{yy} = 2.0071(1), *g*_{zz} = 2.0036(1), *A*_{xx} = 5(2) G, *A*_{yy} = 4(2) G, *A*_{zz} = 31.2(3) G.

Fig. 3b displays the cw X-band EPR spectrum of **2**[•] at room temperature together with its simulation. The isotropic spectrum clearly shows the five lines due to two strongly exchange-coupled ($|2J| \gg |A_{\text{iso}}|$) nitroxide moieties with *S*₁ = *S*₂ = ½ and *I*₁ = *I*₂ = 1 centered at *g*_{iso} = 2.0064(1) and with a splitting of *A*_{iso}/2 = 7.2(1) G. As expected the *A*_{iso}(¹⁴N) values of **2**[•] and **1**[•] are identical. From this EPR spectrum it is not possible to obtain an exact value for the exchange coupling constant *J*, only a lower limit can be estimated [30]. The lowest value for 2*J* which did not cause any significant deterioration of the simulation was 260 G, i.e., $|2J| \geq 260$ G. The anisotropic cw S-band EPR spectrum of a frozen solution of **2**[•] (*T* = 90 K) is depicted in Fig. 3c. The measurement was performed at S-band frequencies to minimize influences of *g* anisotropy on the spectrum. From the width of the spectrum a dipolar coupling constant *D* = 42(3) G was obtained [31]. With that value one can calculate a spin–spin distance of *r*_{ab} = 7.6(2) Å utilizing a simple dipole model

$$r_{\text{ab}}^3 = \frac{\mu_0}{4\pi h} \cdot \frac{g_{\text{iso,a}} \cdot g_{\text{iso,b}} \cdot \mu_{\text{B}}^2}{D} \quad (7)$$

Here, *g*_{iso,a} and *g*_{iso,b} are the isotropic *g* values of electron a and b. The estimated spin–spin distance *r*_{ab} fits nicely to the N–N (7.2 Å) and O–O (8.9 Å) distances from the crystal structure.

For the investigation of the size and sign of the exchange coupling a series of X-band spectra at

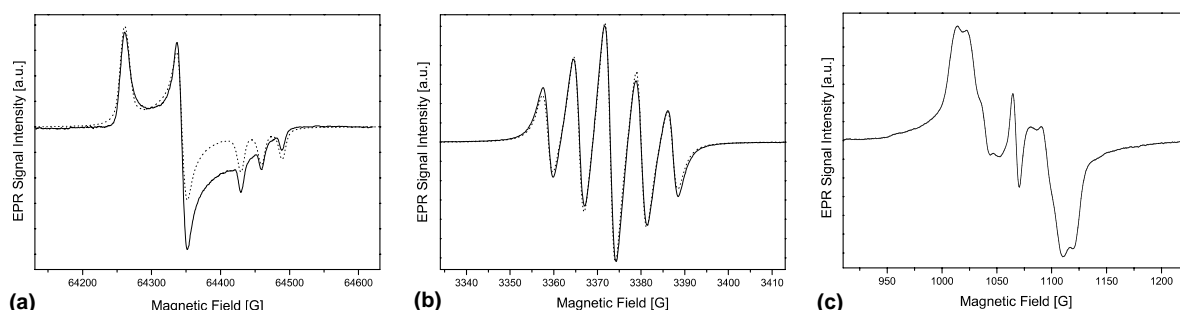


Fig. 3. (a) G-band (180.759 GHz) EPR spectrum of **1**[•] at 10 K. EPR spectra of **2**[•] at (b) X-band frequencies (9.472 GHz) and room temperature; (c) S-band frequencies (2.998 GHz) and 90 K. Simulations are shown as dotted curves.

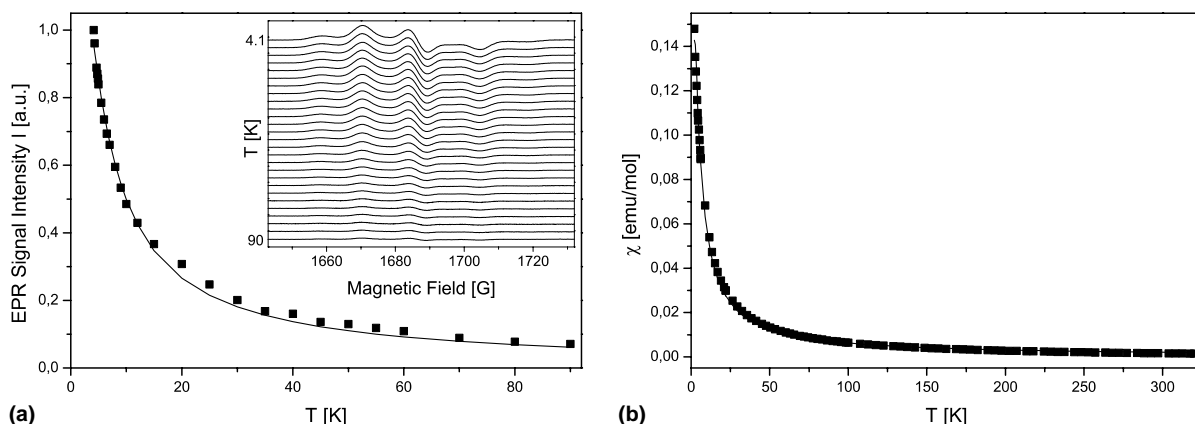


Fig. 4. Temperature dependence of the (a) doubly integrated X-band EPR half-field signal intensity I for $2^{\bullet\bullet}$ in d_8 -toluene (1 mM); (b) magnetic susceptibility χ for a microcrystalline powder of $2^{\bullet\bullet}$ at a constant field of 50 000 Oe. The inset in (a) shows the half-field X-band EPR spectra of $2^{\bullet\bullet}$ at different temperatures. Best fits of the data to Eq. (3) are represented by solid curves.

temperatures from 4.1–90 K were recorded and the doubly integrated EPR half-field signal intensity was plotted against T (Fig. 4a). The best fit of the EPR data according to Eq. (3) leads to $2J = -4.1$ (2) K corresponding to a singlet ground state for $2^{\bullet\bullet}$.

4.3. Magnetic susceptibility measurements

The temperature dependence of the magnetic susceptibility was studied with a SQUID susceptometer (Quantum Design) on a microcrystalline powder of $2^{\bullet\bullet}$ in the temperature range 2–320 K at a magnetic field of 50 000 Oe (Fig. 4b). From best fits of $\chi = f(T)$ with Eq. (3) one obtains $2J = -3.54(4)$ K. At temperatures between 60 and 320 K, χT is constant and equal to 0.7 (emu K)/mol, a value in good agreement with the theoretical value for a system of two isolated $\frac{1}{2}$ spins [5].

5. DFT calculations

5.1. Exchange coupling constant J for $2^{\bullet\bullet}$

For the calculation of the energies of the triplet and broken symmetry state of $2^{\bullet\bullet}$ various basis sets of different sizes were tested. Table 1 displays the results of the unrestricted computations with the B3LYP hybrid functional. The $\langle \hat{S}^2 \rangle$ values show

no serious spin contamination for the triplet calculations and values near one for the BS computations justify the use of Eq. (6) for the calculation of the exchange coupling constant J . From Table 1 it becomes obvious that even a semi-quantitative agreement between theory and experiment can only be achieved with large basis sets of triple- ζ quality including polarization functions. The small double- ζ quality basis sets yield the correct sign of the exchange coupling constant J but show no systematic convergence behavior. For the triple- ζ quality basis sets an increasing number of polarization and diffuse basis functions leads to a convergence towards the experimental data. In all of the computations the singlet state is predicted to be too stable with respect to the triplet state. Compared to other bisnitroxides or organic biradicals [2,32,33] the singlet–triplet separation exhibits an unusually large dependence on the applied basis set. It is inevitable to use polarized triple- ζ quality basis sets in order to obtain reliable exchange coupling values for $2^{\bullet\bullet}$. The results show that it is possible to nearly quantitatively predict $2J$ for $2^{\bullet\bullet}$ with the large 6-311G(df,pd) basis set. Therefore, all of the following calculations were performed using this method. The localized magnetic orbitals of $2^{\bullet\bullet}$ are visualized in Fig. 5a. As expected the SOMOs and therefore also the spin density distribution resemble that of a monomeric TPA unit.

Table 1
Singlet–triplet separation $2J$ computed for 2^{\bullet} and various model systems using unrestricted B3LYP BS DFT methods and comparison with experimental data from this work

System	Method	$2J$ (K)	$\langle \hat{S}^2 \rangle_{\text{BS}}$	$\langle \hat{S}^2 \rangle_{\text{T}}$
2^{\bullet}	6-31G(d)	-265.2	1.0074	2.0074
	6-31+G(d)	-1.3 ^a	1.0090	2.0090
	6-31+G(d,p)	-3852.4	1.0090	2.0090
	6-311G(d)	-37.9	1.0082	2.0082
	6-311G(d,p)	-18.9	1.0082	2.0082
	6-311+G(d)	-12.6	1.0090	2.0090
	6-311G(df,pd)	-6.3	1.0084	2.0084
	SQUID	-3.5		
	EPR	-4.1		
2^{\bullet}_{A}	6-311G(df,pd)	-88.4	1.0083	2.0084
2^{\bullet}_{TS1}	6-311G(df,pd)	-138.9	1.0082	2.0084
2^{\bullet}_{TS2}	6-311G(df,pd)	0.0	1.0084	2.0084
2^{\bullet}_{TS3}	6-311G(df,pd)	0.0	1.0072	2.0072

^a Energy difference below $10^{-5} E_{\text{h}}$.

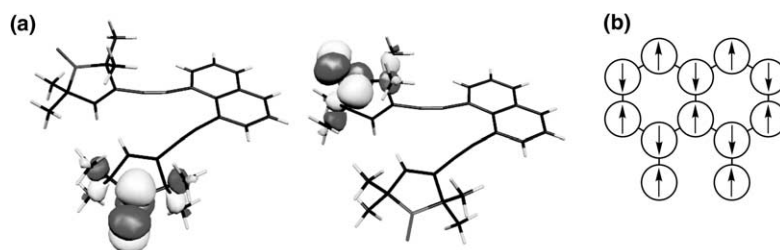


Fig. 5. (a) Singly occupied magnetic orbitals of 2^{\bullet} . (b) Spin polarization pattern for 1,8-substituted naphthalene bridges mediating ferromagnetic exchange coupling via the π -network.

5.2. Exchange coupling constant J for model systems

After the successful computation of $2J$ for 2^{\bullet} further efforts were made to unravel the mechanisms of the exchange interaction. For this purpose calculations on four model systems 2^{\bullet}_{A} , 2^{\bullet}_{TS1} , 2^{\bullet}_{TS2} and 2^{\bullet}_{TS3} (Fig. 1b) were performed. In these models the distance and relative orientation of the two nitroxide moieties were taken from the crystal structure of 2^{\bullet} . Then the aromatic naphthalene ring system was replaced by an alkyl chain (2^{\bullet}_{A}) or completely deleted (2^{\bullet}_{TS1}). Furthermore, the two acetylene units were omitted in 2^{\bullet}_{TS2} and 2^{\bullet}_{TS3} simply consists of two H_2NO molecules. When necessary hydrogen atoms were added with standard bond lengths and angles. Table 1 displays the obtained values for the singlet–triplet splitting $2J$

when using the UB3LYP/6-311G(df,pd) combination. For 2^{\bullet}_{A} and 2^{\bullet}_{TS1} $2J$ becomes more negative, i.e., the omission of the π -system or of the whole bridge both lead to a much stronger antiferromagnetic interaction of -88.4 and -138.9 K, respectively. 2^{\bullet}_{TS2} and 2^{\bullet}_{TS3} show no magnetic interaction as is expected for two nitroxide radicals separated by a distance of $\sim 7\text{--}8$ Å and interacting only through space [2].

6. Discussion

A comparison of the antiferromagnetic exchange coupling constants J for 2^{\bullet} from EPR ($2J = -4.1$ K) and from magnetic susceptibility measurements ($2J = -3.54$ K) shows very good agreement. Since the EPR measurements were

performed on diluted solutions and $2J$ from these measurements resembles the result from the SQUID measurements, it can be deduced that 2^{\bullet} represents in fact an intramolecular exchange-coupled bisnitroxide system and that intermolecular interactions can be neglected. This is also in agreement with the shortest intermolecular NO–NO distances of 5 Å found in the unit cell of the crystal. For such a distance in combination with the observed relative orientation of these nitroxide moieties a vanishing magnetic interaction is expected [2]. Furthermore, the spin–spin distance of 7.6 Å acquired from the frozen solution EPR spectrum also shows that the structure of 2^{\bullet} in solution is comparable to the structure in the crystal.

The DFT calculations ($2J = -6.3$ K) support the experimental data and furthermore provide insight into the exchange mechanisms for 2^{\bullet} . The result of the computation on the model system where the naphthalene unit is deleted (2^{\bullet}_{TS1}) should reveal those contributions to J that are only due to intramolecular through-space interactions. The value of $2J = -138.9$ K shows that the total exchange coupling through space is strongly antiferromagnetic. Considering that for 2^{\bullet}_{TS2} and 2^{\bullet}_{TS3} which represent through-space interactions between the two five-membered nitroxide rings or the N–O groups themselves no magnetic interaction was found, it can be concluded that the strong antiferromagnetic interaction of -138.9 K is solely due to a through-space coupling via the two acetylene units. The small distance of 2.89 Å between the triple bonds is close enough to allow through-space interactions of these π -orbitals. The model system 2^{\bullet}_{A} with the alkyl chain as linking bridge instead of naphthalene should include through-space coupling and additionally through-bond interactions via the alkyl linker. The exchange coupling of $2J = -88.4$ K for 2^{\bullet}_{A} is less negative compared to 2^{\bullet}_{TS1} . What is interesting about 2^{\bullet}_{A} is the fact that including all interaction pathways except the one through the π -system of the naphthalene bridge, it is not possible to model the small antiferromagnetic exchange interaction experimentally and theoretically found for 2^{\bullet} . Therefore it becomes obvious that the naphthalene unit mediates a ferromagnetic through-bond interaction of

the same order of magnitude as the antiferromagnetic through-space coupling. This ferromagnetic coupling through the π -system can be explained by the 1,8-substitution pattern which resembles the *meta*-benzene substitution. Such a *meta* substitution is known to evoke ferromagnetic interactions [32] which can be rationalized using a simple spin polarization picture of the π -system (Fig. 5b). The surprisingly strong antiferromagnetic and ferromagnetic exchange couplings calculated can be understood by assuming an effective coupling of the magnetic N–O π -orbitals to the π -system of the bridge via a superexchange mechanism [34]. This is supported by the close distance of 2.2 Å between the nitrogen of the N–O unit and the center of the double bond of the pyrroline ring. A delocalization of spin density into the bridge can be excluded since a hyperfine coupling to the vinyl hydrogen could not be observed by EPR and a negligible spin density was found at this H in the calculations. The sum of the ferromagnetic through-bond interaction and the short-circuit through-space interaction via the acetylene groups finally leads to the observed small antiferromagnetic coupling for 2^{\bullet} .

7. Conclusions

We synthesized and structurally characterized the new bisnitroxide 2^{\bullet} in which two nitroxide moieties are coupled via a 1,8-substituted naphthalene bridge. Temperature-dependent EPR and susceptibility measurements on 2^{\bullet} both revealed an antiferromagnetic exchange coupling $2J$ of -4.1 and -3.54 K, respectively.

DFT calculations with the large 6-311G(df,pd) basis set using the geometry of the crystal structure of 2^{\bullet} gave $2J = -6.3$ K in good agreement with the experiment. The intramolecular exchange coupling mechanisms contributing to J were analyzed by using DFT calculations on model systems. These theoretical investigations showed that the short-circuit through-space coupling via the acetylene groups is strongly antiferromagnetic ($2J = -138.9$ K) and that the coupling of the two spins through the π -system of the naphthalene bridge is ferromagnetic and of the same order of magnitude, resulting in the weak observed spin–

spin coupling. The coupling of the spin-bearing N–O groups to the bridge is suggested to take place via a superexchange mechanism.

Acknowledgements

This work was financially supported by the DFG. J. F. gratefully acknowledges the Fonds der Chemischen Industrie for a *Chemiefondsstipendium für Doktoranden* and O. S. the DFG for a *Habilitandenstipendium*. Thanks to B. Wolf for the SQUID measurements, M. Bolte for the X-ray measurements and to I. Ciofini for the helpful discussion. The authors also thank T. F. Prisner for his support.

References

- [1] D. Gatteschi, O. Kahn, J.S. Miller, F. Palacio (Eds.), *Magnetic Molecular Materials*, NATO ASI Series, Kluwer Academic Publishers, Dordrecht, 1991.
- [2] K. Yamaguchi, M. Okumura, J. Maki, T. Noro, H. Namimoto, M. Nakano, T. Fueno, K. Nakasuji, *Chem. Phys. Lett.* 190 (1992) 353.
- [3] V. Barone, A. Bencini, A. di Matteo, *J. Am. Chem. Soc.* 119 (1997) 10831.
- [4] C. Elschenbroich, O. Schiemann, O. Burghaus, K. Harms, *J. Am. Chem. Soc.* 119 (1997) 7452.
- [5] O. Kahn, *Molecular Magnetism*, first ed., VCH, Weinheim, 1993.
- [6] V. Barone, A. di Matteo, F. Mele, I. de P. R. Moreira, F. Illas, *Chem. Phys. Lett.* 302 (1999) 240.
- [7] J. Comarmond, P. Plumeré, J.M. Lehn, Y. Agnus, R. Louis, R. Weiss, O. Kahn, I. Morgestern-Badarau, *J. Am. Chem. Soc.* 104 (1982) 6330.
- [8] N. Arulsamy, J. Glerup, D.J. Hodgson, *Inorg. Chem.* 33 (1994) 2066.
- [9] N.L. Frank, R. Clérac, J.-P. Sutter, N. Daro, O. Kahn, C. Coulon, M.T. Green, S. Golhen, L. Ouahab, *J. Am. Chem. Soc.* 122 (2000) 2053.
- [10] A. Cogne, J. Laugier, D. Luneau, P. Rey, *Inorg. Chem.* 39 (2000) 5510.
- [11] B. Bleaney, K.D. Bowers, *Proc. Roy. Soc. (London) Ser. A* 214 (1952) 451.
- [12] S. Gambarelli, D. Jaouen, A. Rassat, L.-C. Brunel, C. Chachaty, *J. Phys. Chem.* 100 (1996) 9605.
- [13] R.G. Parr, W. Yang, *Density-Functional Theory of Atoms and Molecules*, first ed., Oxford University Press, New York, 1989.
- [14] A. di Matteo, V. Barone, *J. Phys. Chem. A* 103 (1999) 7676.
- [15] L. Noodleman, *J. Chem. Phys.* 74 (1981) 5737.
- [16] R. Caballol, O. Castell, F. Illas, I. de P. R. Moreira, J.P. Malrieu, *J. Phys. Chem. A* 101 (1997) 7860.
- [17] A.A. Ovchinnikov, J.K. Labanowski, *Phys. Rev. A* 53 (1996) 3946.
- [18] Y. Takano, T. Soda, Y. Kitagawa, Y. Yoshioka, K. Yamaguchi, *Chem. Phys. Lett.* 301 (1999) 309.
- [19] C. Desplanches, E. Ruiz, A. Rodriguez-Forteza, S. Alvarez, *J. Am. Chem. Soc.* 124 (2002) 5197.
- [20] M.J. Frisch et al., *GAUSSIAN 98 (Revision A.7)*, Gaussian, Inc., Pittsburgh PA, 1998.
- [21] J.B. Foresman, Æ. Frisch, *Exploring Chemistry with Electronic Structure Methods*, second ed., Gaussian Inc., Pittsburgh, PA, 1996.
- [22] A.D. Becke, *J. Chem. Phys.* 98 (1993) 5648.
- [23] P.J. Stephens, F.J. Devlin, C.F. Chabalowski, M.J. Frisch, *J. Phys. Chem.* 98 (1994) 11623.
- [24] A. Spaltenstein, B.H. Robinson, P.B. Hopkins, *Biochemistry* 28 (1989) 9484.
- [25] H.O. House, D.G. Koepsell, W.J. Campbell, *J. Org. Chem.* 37 (1972) 1003.
- [26] T. Strube, Ph.D. Thesis, Frankfurt, 2002.
- [27] A. Weber, O. Schiemann, B. Bode, T.F. Prisner, *J. Magn. Reson.* 157 (2002) 170.
- [28] M. Rohrer, O. Brüggemann, B. Kinzer, T.F. Prisner, *Appl. Magn. Reson.* 21 (2001) 257.
- [29] J. Eloranta, XEMR 0.7, <ftp://epr.chem.jyu.fi/pub/xemr/>.
- [30] C. Elschenbroich, O. Schiemann, O. Burghaus, K. Harms, J. Pebler, *Organometallics* 18 (1999) 3273.
- [31] G.R. Eaton, S.S. Eaton, in: L.J. Berliner, J. Reuben (Eds.), *Biological Magnetic Resonance*, vol. 8, Plenum Press, New York, 1989, p. 339.
- [32] M. Mitani, H. Mori, Y. Takano, D. Yamaki, Y. Yoshioka, K. Yamaguchi, *J. Chem. Phys.* 113 (2000) 4035.
- [33] R. Improta, K.N. Kudin, G.E. Scuseria, V. Barone, *J. Am. Chem. Soc.* 124 (2002) 113.
- [34] H.M. McConnell, *J. Chem. Phys.* 35 (1961) 508.